p-^{6}Li Ignition and Multipoles as Advanced Fuel Cycle Reactors

R.W. Conn and G. Shuy

September 25, 1978

UWFDM-262

FUSION TECHNOLOGY INSTITUTE

UNIVERSITY OF WISCONSIN

MADISON WISCONSIN

p-^{6}Li Ignition and Multipoles as Advanced Fuel Cycle Reactors

R.W. Conn and G. Shuy

Fusion Technology Institute
University of Wisconsin
1500 Engineering Drive
Madison, WI 53706

http://fti.neep.wisc.edu

September 25, 1978

UWFDM-262

p-^{6}Li Ignition and Multipoles as Advanced Fuel Cycle Reactors

R. W. Conn

G. Shuy

September 25, 1978

Fusion Research Program
Nuclear Engineering Department
University of Wisconsin
Madison, Wisconsin 53706

TABLE OF CONTENTS

	PAGE
Abstract	i
I. Introduction - Advanced Fuel Fusion Reactors	1
II. Advanced Fuel Cycles	4
A. Proton Based Cycles	4
B. Deuterium Based Cycles	10
III. The Fully Chain Reacted p-^{6}Li Fuel Cycle	14
A. Reactivity of p-^{6}Li Chain Reaction	14
B. Energy Balance and Q Values	15
IV. Multipoles as Reactors for Advanced Fuels	17
A. Octopole Coil Design	23
B. Power Cycle Considerations and Plasma Q Values	32
V. Future Directions in Experiments and Physics Suggested by Reactor Considerations.	38

Abstract

We show that the fully chain reacted p-^{6}Li cycle can achieve ignition against bremsstrahlung when $T_e \sim 150$ keV and $T_i \sim 250$ keV. The excess power over ignition can be as large as 20 times the bremsstrahlung when T_i is 500 keV. At 300 keV, the plasma can have $n\tau_E^e$ equal to 3×10^{14} cm^{-3}-s and still achieve ignition. Octopoles and higher order multipoles are confinement approaches ideally suited for advanced fuels because of the low central B field which helps minimize synchrotron emission. The advantages of proton based fusion reactors include no gaseous radioactivity or fuel breeding, no neutron radiation damage to materials, improved system maintainability and, potentially, improved reliability, very low levels of induced radioactivity (governed by side reactions and (γ,n) reactions), and simplified blanket design. Since all the heat is generated as a surface heat load, such a reactor is the fusion equivalent of a coal-fired boiler. The physics and technical difficulties are described in the context of appropriate next steps in a multipole advanced fuel development program.

I. Introduction - Advanced Fuel Fusion Reactors

Fusion devices utilizing the D-T-Li fuel cycle will certainly be the first to demonstrate energy breakeven and also very likely the first to demonstrate commercial fusion reactors. The requirements for ion temperature and energy confinement are perhaps an order of magnitude lower then the requirements for other fuel cycles. Nevertheless, the ultimate goal of fusion power is to achieve a reactor based on an inherently neutronless fuel cycle that insures an inexhaustible fuel supply. To preserve this potential, it is essential to maintain efforts to develop advanced fuel cycle fusion power, especially with fuel cycles based on protons. The elimination of deuterium is the key to a truly neutronless reactor. On the path to this ultimate goal, deuterium based fuel cycles such as D-D and D-^{3}He can play a substantial role. They can be used for example as fuels in test reactors between a proof-of-principle device and a truly proton based fusion system. The reason is that the T_i and $n\tau_E$ requirements of D-D and D-^{3}He are intermediate between those of D-T and those of a proton based fuel cycle.

The advanced fuel cycle of choice is the catalyzed and fully chain reacted p-^{6}Li cycle which involves the reactions

$$p + {}^6Li \rightarrow {}^3He + {}^4He \qquad Q = 4 \text{ MeV}$$

$$^3He + {}^6Li \rightarrow \bar{\bar{p}} + 2{}^4He \qquad Q = 16.8 \text{ MeV}$$

$$^3He + {}^3He \rightarrow 2\bar{p} + {}^4He. \qquad Q = 12.9 \text{ MeV}$$

The fast protons, $\bar{\bar{p}}$ and $\bar{p}$, have a substantial probability of reacting with ^{6}Li prior to thermalization when the electron temperature, T_e, exceeds 100 keV. Accounting fully for the chain reaction (as in a fission reactor cycle), this cycle will ignite against bremsstrahlung losses when T_i exceeds about 250 keV.

The margin over ignition against bremsstrahlung can be substantial for T_i = 300-500 keV. All this is discussed shortly but is mentioned here to provide a framework for describing the potential advantages of a proton based fusion reactor.

The potential advantages of a proton based fusion reactor are substantial and are summarized on Table 1. Firstly, both fuels in cycles such as p-^{6}Li are abundant. Secondly, there is no gaseous radioactivity and no need to breed tritium. This allows distinct flexibility in blanket design. The elimination of tritium eliminates problems of tritium management and eliminates in many cases the need for an intermediate loop in the power cycle. Thirdly, there is no neutron radiation damage to materials. This will impact favorably via improved system maintainability, availability and reliability. Some neutron induced radioactivity may result from a very small number of side reactions but this depends on branching ratios. This, together with the absence of gaseous radioactivity, provides particular environmental impact advantages that will affect costs, licensing and siting. Fourthly, although the plasma power density is likely to be lower than in a D-T reactor with the same β value, the size limitations imposed by the neutron wall loading in D-T systems does not permit one to take full advantage of very high β in D-T. With a neutronless advanced fuel, magnets can be closer to the reaction chamber to offset the need for somewhat higher fields.
The blanket amounts to nothing more than the chamber itself since the energy is released primarily as electromagnetic radiation.

In short, a proton based fusion reactor would be the fusion analog of a coal fired boiler where the power is provided essentially as a surface heat

Table 1

Potential Advantages of Proton-Based Fusion Reactors
(Particularly p-^{6}Li)

1. Fuels are essentially inexhaustible.
2. No gaseous radioactivity.
3. No fuel breeding requirement.
4. Simple blanket design - blanket is now just a first wall.
5. No radiation damage to structural materials.
6. Safety aspects similar to coal plants, not nuclear power.
7. Improved system maintainability and thus, potentially, improved reliability and availability.
8. Very low levels of induced radioactivity (governed by side reactions and branching ratios).
9. Potentially low environmental impact on air pollution, mining, and long term solid waste disposal.
10. Potential for good systems economics.
    A. Balance of plant costs should be similar to coal plant. Nuclear oriented subsystems are eliminated.
    B. Fuel costs will be less than for nuclear.
    C. Fusion island costs can be greater than for nuclear.
    D. No intermediate loop required for safety.

load. Cost advantages can be gained by eliminating systems like intermediate heat exchangers, tritium extraction, tritium cleanup, radioactive waste control and remote handling. Potential environmental advantages can minimize licensing and siting issues. These cost savings can be used to a degree to offset disadvantages such as lower plasma power density.

II. Advanced Fuel Cycles

A. Proton Based Cycles

Two advanced fuel cycles, p-^{11}B and p-^{6}Li, meet the neutronless criterion. The reaction

$$p + {}^{11}B \rightarrow 3\alpha \qquad Q = 8.68 \text{ MeV} \tag{1}$$

has been considered by Dawson,[1] Cordey,[2] and Conn et al.[3] It is found using the reaction rate parameter derived from recently measured $^{11}B(p,\alpha)2\alpha$ cross section data that the maximum possible plasma Q value is $\lesssim 1$. Q is defined as

$$Q = P_F/P_{inj} \tag{2}$$

where P_F is the total fusion power and P_{inj} is the power externally injected into the plasma.

The p-^{6}Li cycle has also been considered by several authors, particularly Cordey and McNally.[4] Cordey predicted that the maximum Q value for this cycle is ~3. However, he did not completely include the fact that the p-^{6}Li cycle is a chain reaction cycle. As we will show, the potential for achieving ignition against bremsstrahlung (i.e. $P_F > P_x$ where P_x is the bremsstrahlung power loss) with the p-^{6}Li cycle is good. In certain cases, we find P_F/P_x as large as 20.

The first reaction in this cycle is

$$p + {}^{6}Li \rightarrow {}^{3}He + {}^{4}He \qquad Q = 4 \text{ MeV} \tag{3}$$

where the cross section is shown in Fig. 1 and the reaction parameter $\langle\sigma v\rangle_{16}$ is shown in Fig. 2. The product ^3He is reactive with ^6Li and the reaction is

$$^3He + {}^6Li \xrightarrow{90\%} p\ (11.3\ MeV) + 2\alpha \qquad Q = 16.8\ MeV$$
$$^3He + {}^6Li \xrightarrow{10\%} p\ (14.9\ MeV) + {}^8Be \qquad Q = 16.8\ MeV \tag{4}$$

A branch with less than 1% probability produces d + ^7Be. The burning of this small deuterium content will be primarily by the reactions

$$D + {}^3He \rightarrow p(14.7\ MeV) + \alpha \qquad Q = 18.3\ MeV$$
and
$$D + {}^6Li \rightarrow \{\text{several branches; neutrons are produced.}\} \tag{5}$$

The burn is however extremely lean in D. If n_3 exceeds n_6, as is likely, then the higher reactivity of D-^3He will cause this neutronless reaction to dominate.

The ^3He-^6Li reaction produces a fast proton which can in turn react with ^6Li thereby initiating a chain reaction. Since the electron temperature for this cycle will exceed 100 keV, the probability of fast protons fusing with ^6Li, denoted P_{16}, can be quite high. Values of P_{16} are shown in Figs. 3 and 4 as a function of the ^6Li to proton density ratio and T_e for two different values of T_i.

Since ^3He is an intermediate product, one must also include the possibility of the reaction

$$^3He + {}^3He \rightarrow 2p(5.2\ MeV) + \alpha \qquad Q = 12.8\ MeV \tag{6}$$

which, while consuming two ^3He atoms, produces two fast protons. These protons can again react with ^6Li to maintain the chain reaction.

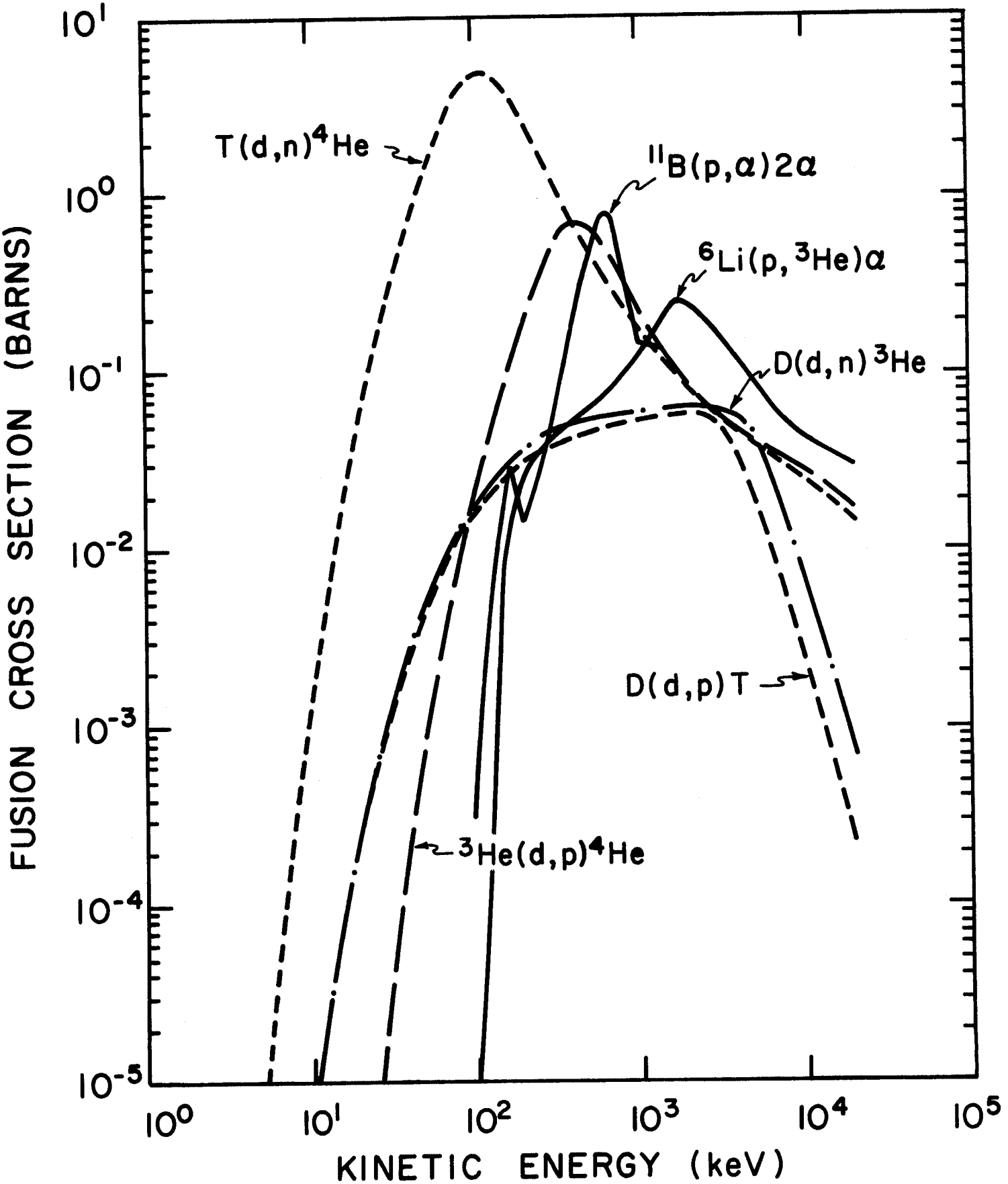
FUSION CROSS SECTION (BARNS)
KINETIC ENERGY (keV)
T(d,n)⁴He
¹¹B(p,α)2α
⁶Li(p,³He)α
D(d,n)³He
D(d,p)T
³He(d,p)⁴He
10¹
10⁰
10⁻¹
10⁻²
10⁻³
10⁻⁴
10⁻⁵
10⁰
10¹
10²
10³
10⁴
10⁵

FIGURE 1

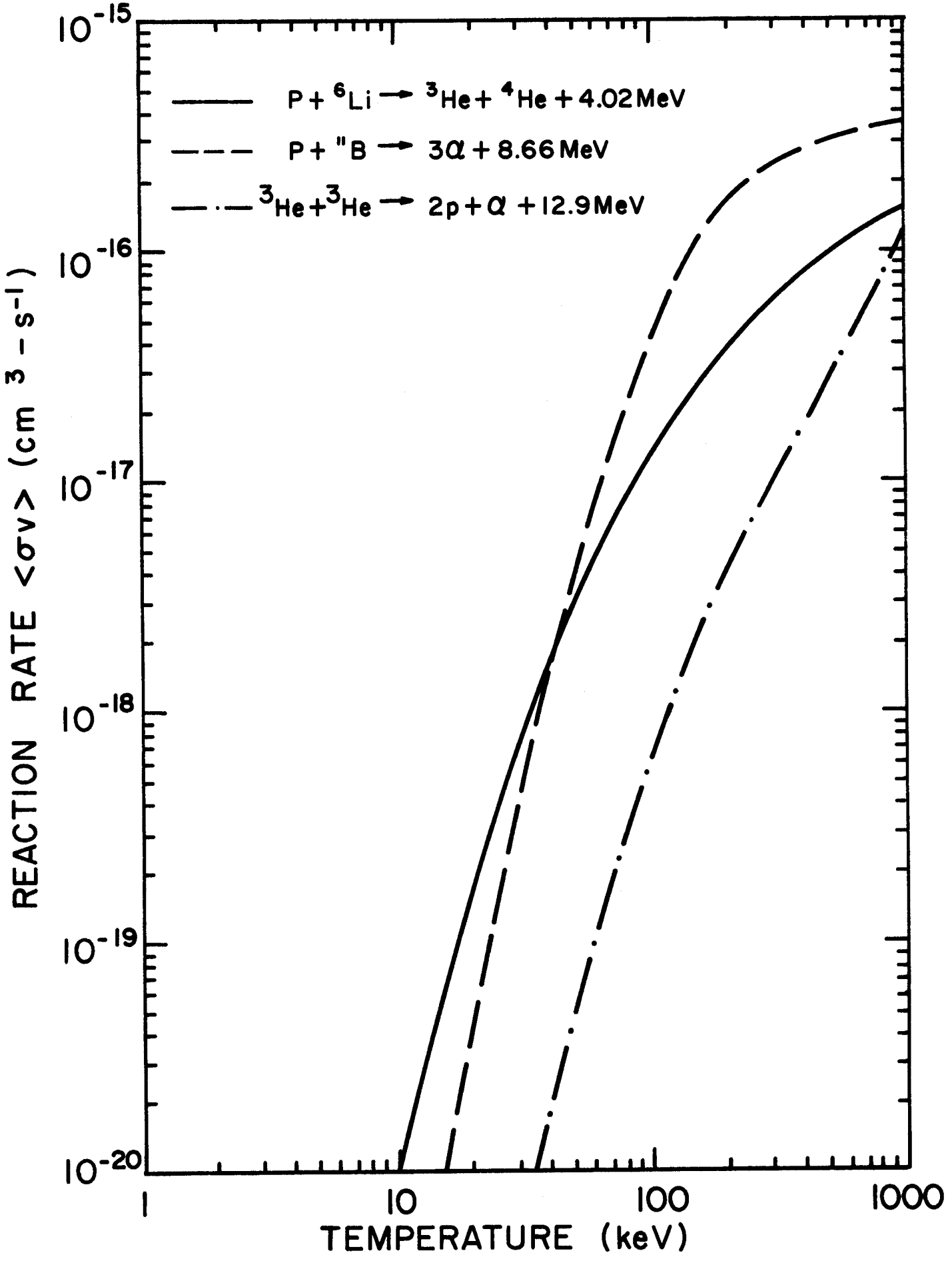
P + ^{6}Li → ^{3}He + ^{4}He + 4.02 MeV
P + ^{11}B → 3α + 8.66 MeV
^{3}He + ^{3}He → 2p + α + 12.9 MeV
REACTION RATE <σv> (cm^{3} - s^{-1})
10^{-15}
10^{-16}
10^{-17}
10^{-18}
10^{-19}
10^{-20}
1
10
100
1000
TEMPERATURE (keV)

FIGURE 2

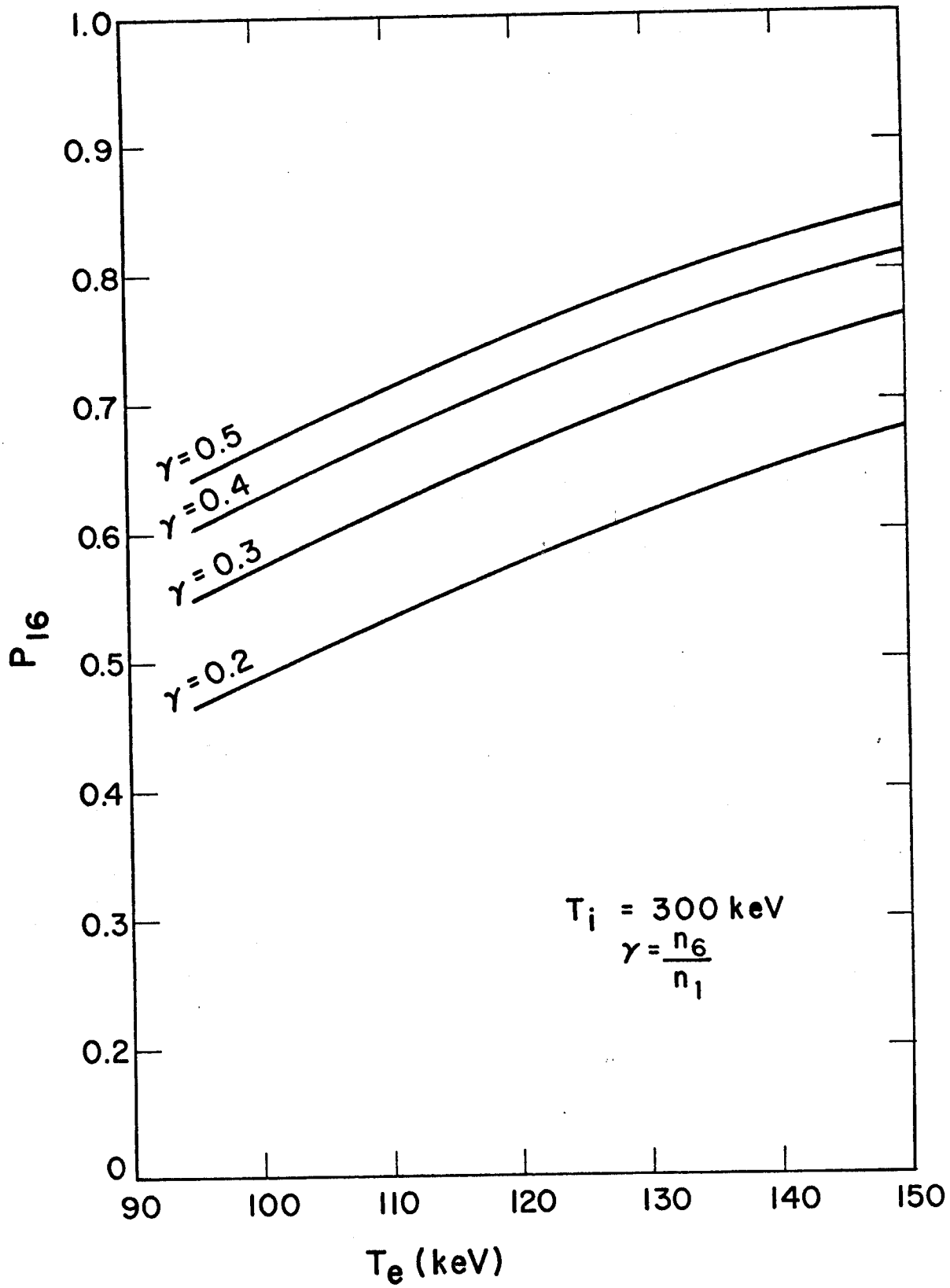

Fig. 3. The probability of fast protons (E_o=12 MeV) fusing with ^6Li prior to slowing down. $\gamma=n_6/n_1$, the ^6Li to proton density ratio. T_i=300 keV.

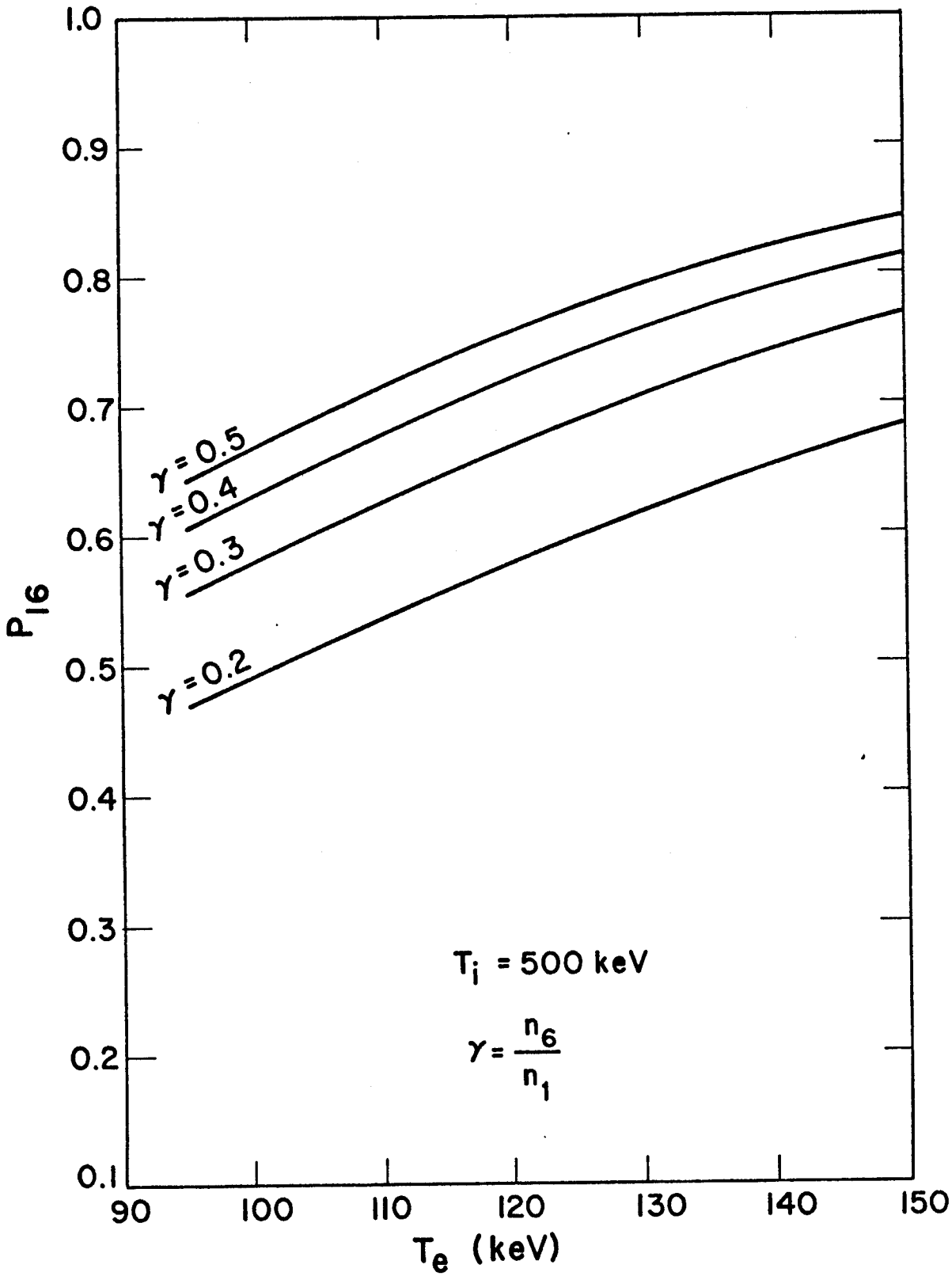

Fig. 4. The probability of fast proton fusion with ^{6}Li prior to slowing down.

The reactions (3), (4) and (6) are the key elements of the p-^{6}Li chain reaction cycle. Since there is a one-to-one correspondence between the production and consumption of protons, it would not appear that a super-critical chain reaction could occur. However, fast protons have a sizable cross section for nuclear elastic scattering via p-p reactions. In the process, two relatively fast protons can be generated, each of which can still have a reasonable probability for reaction with ^{6}Li. In such an event, nuclear elastic scattering would enhance the mixture reactivity still further and could lead to a prompt critical chain. Initial results shown in Fig. 4a show that indeed, P_{16} can exceed 1 so that a prompt critical chain can occur. This particular effect is under active investigation but is not included in the results to be reported here.

B. Deuterium Based Cycles

The two major advanced fuel cycles based on deuterium are D-D and D-^{3}He. The D-D reaction is

$$D + D \xrightarrow{50\%} p + T \qquad D + D \xrightarrow{50\%} n + {}^3He \qquad (6\text{-}1)$$

and the product T and ^{3}He, when burned, add additional energy, albeit with an additional neutron at an energy of 14 MeV. D-D and catalyzed D-D do not require tritium breeding blankets but do produce about as many neutrons per unit energy as D-T.

The D-^{3}He reaction is

$$D + {}^3He \rightarrow p + {}^4He \qquad Q = 18.35 \text{ MeV} \qquad (6\text{-}2)$$

where both reaction products are charged particles. Neutrons are thus produced only from side D-D reactions and the number can be made relatively small by burning lean in D.

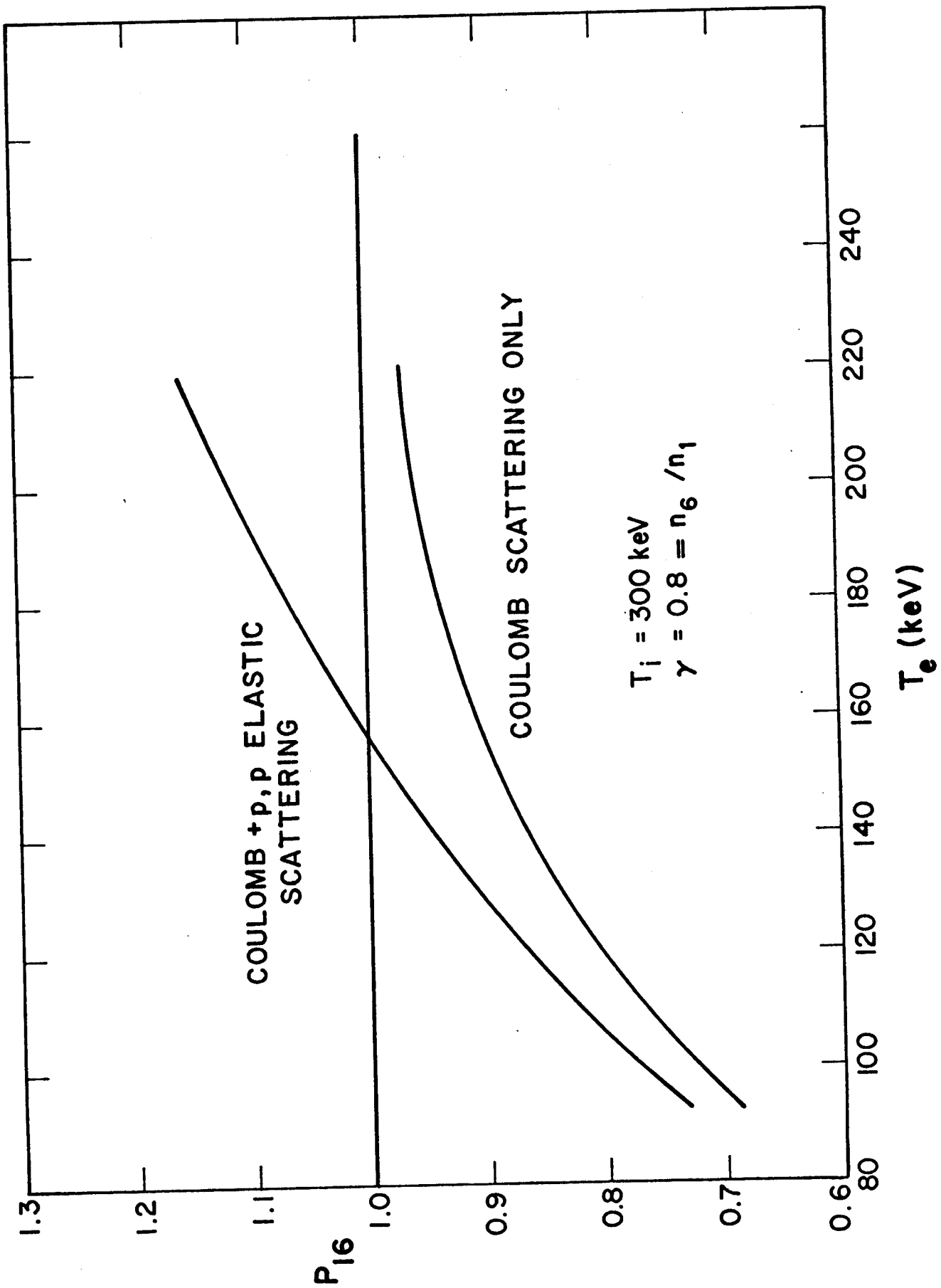
COULOMB + p,p ELASTIC SCATTERING
COULOMB SCATTERING ONLY
T_i = 300 keV
$\gamma = 0.8 = n_6 / n_1$
P_{16}
T_e (keV)
1.3
1.2
1.1
1.0
0.9
0.8
0.7
0.6
80
100
120
140
160
180
200
220
240

Fig. 4a

A thorough analysis can be done of the T_i, T_e, $n\tau_E$ requirements of this cycle using a global plasma energy balance model. One finds the results shown in Figs. 5, 6 and 7. For $T_i \sim 75$ keV, one can achieve Q~1 with T_e~40keV, $n\tau_E \sim 0.5\text{-}1.0 \times 10^{15}\text{cm}^{-3}\text{-s}$, and $n\tau_E^e \sim 10^{14}\text{cm}^{-3}\text{-s}$. Interestingly, at these conditions, a D-T fuel mixture would be ignited and have $Q = \infty$. It is of interest to point out the possibility of simulating D-T burn in the so-called Hot Ion Mode or Maxwellian Fusion Amplifier (MFA) mode using D-^{3}He. The reason is that D-^{3}He experiments need not have extensive tritium handling facilities nor would the reactors become overly radioactive. The tritium and neutrons produced by side D-D reactions can be controlled by operating on a lean D mixture of D and ^{3}He. Also, the fusion energy released in charged particles per D-^{3}He reaction is roughly five times that released in a D-T reaction. Therefore, a Q of 0.2 for D-^{3}He is equivalent to Q=1 for D-T in terms of the charged particle reaction product heating of the plasma. One could therefore study many of the burn dynamic and microinstability problems associated with MFA operation without using D-T. The magnetic container required would have to be relatively high β ($\beta \gtrsim 20\%$) to allow the operating temperature to approach 50 keV and it would have to exhibit good ion energy confinement. For $Q = 0.2$, $n\tau_E^i$ must be $\sim 10^{14}\text{cm}^{-3}\text{-s}$ and $n\tau_E^e \sim 10^{13}\text{-s}$.

The plasma characteristics required to achieve adequate Q in D-^{3}He are somewhat less restrictive than those for p-^{6}Li. The $n\tau_E^e$ can be about $10^{14}\text{cm}^{-3}\text{-s}$, T_i can be 75-100 keV and T_e can be 30-50 keV. This suggests the D-^{3}He can also play a <u>crucial</u> role in <u>advanced fuel cycle reactor development</u> by being the fuel to use in the first reactors to follow the proof-of-principle experiment. Such reactors would be intermediate burning physics experiments (there may

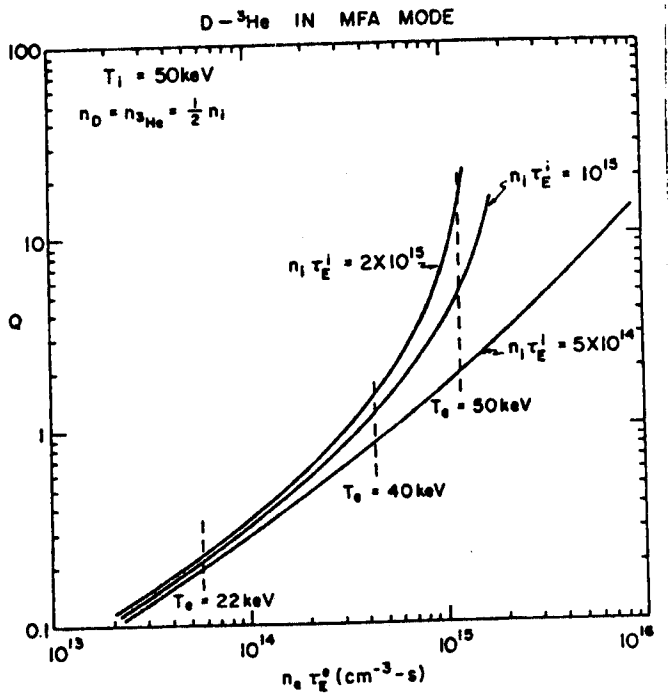

FIGURE 5

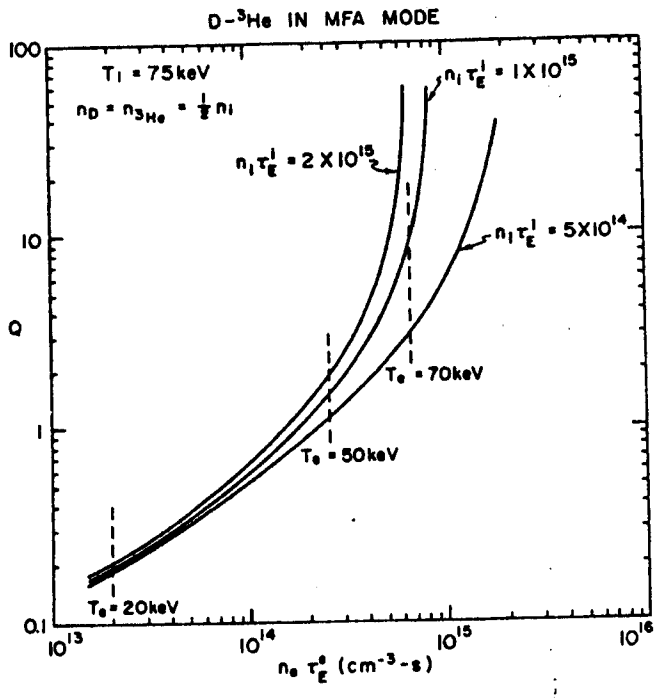

FIGURE 6

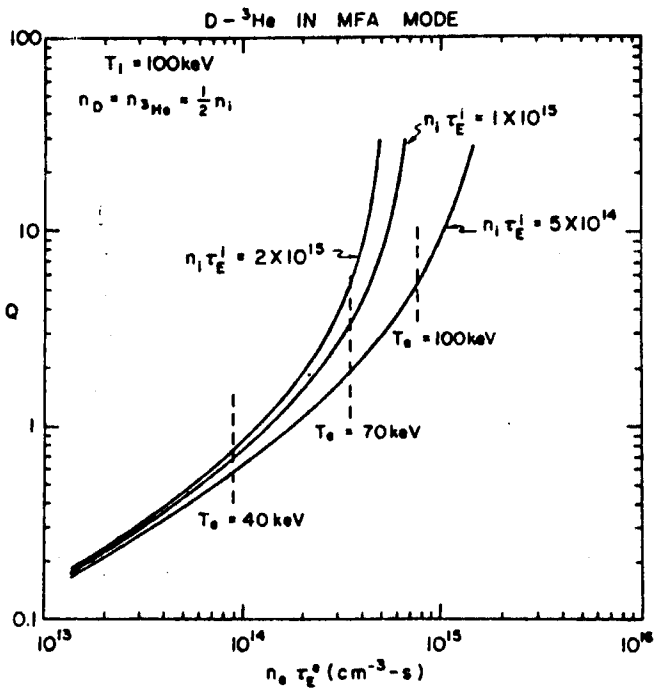
D – ^{3}He IN MFA MODE
T_i = 100keV
$n_D = n_{^3He} = \frac{1}{2} n_i$
$n_i \tau_E^i = 1 \times 10^{15}$
$n_i \tau_E^i = 2 \times 10^{15}$
$n_i \tau_E^i = 5 \times 10^{14}$
T_e = 100keV
T_e = 70keV
T_e = 40keV
Q
100
10
1
0.1
10^{13}
10^{14}
10^{15}
10^{16}
$n_e \tau_E^e$ (cm^{-3}-s)

FIGURE 7

only be the need for one) on the way to a proton-based advanced fuel reactor. One should learn essentially all pertinent physics information in these intermediate burning physics experiments.

III. The Fully Chain Reacted p-^{6}Li Fuel Cycle

A. Reactivity of p-^{6}Li Chain Reaction

The Maxwellian fusion reaction rate for the reaction of eqn. (3) is

$$a_{16} = n_1 n_6 \langle\sigma v\rangle_{16} \tag{7}$$

where n_1 is the proton density and n_6 is the ^{6}Li density. Each reaction produces one ^{3}He. Let P_{16} be the probability that a fast proton produced in a ^{3}He-^{6}Li reaction will fuse prior to slowing down. Let $\bar{P}_{16}$ be the comparable quantity for protons produced from ^{3}He-^{3}He reactions. Then the total production rate of ^{3}He is

$$P_3 = \frac{a_{16} + a_{36} P_{16} + a_{33} \bar{P}_{16}}{1 - (P_{36}P_{16} + P_{33}\bar{P}_{16})} \tag{8}$$

where

$$a_{36} = n_3 n_6 \langle\sigma v\rangle_{36} \tag{8a}$$

and

$$a_{33} = n_3^2 \langle\sigma v\rangle_{33}. \tag{9}$$

n_3 is the ^{3}He density, $\langle\sigma v\rangle_{36}$ is the ^{3}He-^{6}Li reaction rate parameter and $\langle\sigma v\rangle_{33}$ is the ^{3}He-^{3}He reaction rate parameter. The consumption rate of ^{3}He is

$$C_3 = \frac{a_{36} + a_{33} + a_{16}(P_{36}+P_{33}) + (a_{36}P_{33} - a_{33}P_{36})(P_{16} - \bar{P}_{16})}{1 - (P_{36}P_{16} + P_{33}\bar{P}_{16})}. \tag{10}$$

Let us consider the simple case where we neglect the ^{3}He-^{3}He reaction so that $a_{33} = P_{33} = 0$. In this limit we find

$$P_3 = \frac{a_{16} + a_{36} P_{16}}{(1 - P_{36} P_{16})} \tag{11}$$

and

$$C_3 = \frac{a_{36} + A_{16} P_{36}}{(1 - P_{36} P_{16})} \quad . \tag{12}$$

The equilibrium ^3He content is then

$$n_3 = n_1 \frac{\langle\sigma v\rangle_{16}}{\langle\sigma v\rangle_{36}} \frac{(1 - P_{36})}{(1 - P_{16})} \tag{13}$$

and the fusion power output is

$$P_F = n_1 n_6 \langle\sigma v\rangle_{16} \left(\frac{1}{1-P_{16}}\right)(Q_{16} + Q_{36}) \tag{14}$$

where Q_{16} and Q_{36} are the nuclear reaction Q values for the respective reactions. Note that this fusion power is considerably enhanced over the uncatalyzed, non-chain reaction that results from considered only p-^{6}Li. In the later case, P_F would simply be $n_1 n_6 \langle\sigma v\rangle_{16} Q_{16}$. As we have shown P_{16} can readily exceed 0.5. In this case, P_F from eqn. (14) is 10 times that for the base reaction, eqn. (3). Also, note that n_3 does not enter directly the expression for P_F. The reason is that in equilibrium, the reactivity is enchanced by $Q_{16}+Q_{36}$ and by $(1-P_{16})^{-1}$. The latter factor comes from summing over all generations in which case any dependence on n_3 should disappear.

B. Energy Balance and Q Values

The simplest energy balance that one may use to assess the potential of the fully chain reacted p-^{6}Li cycle is to find the ratio of fusion power to bremsstrahlung in the case where the fusion power deposited in the ions balances election-ion rethermalization. Bremsstrahlung radiative power is given by

$$P_x = 2.94 \times 10^{-15} n_e^2 Z_{eff} T_e^{1/2} (1+\eta) (keV/cm^3\text{-}s) \tag{15}$$

where

$$Z_{eff} = \sum_j n_j Z_j^2 / n_e, \tag{16}$$

and the sum extends over all ion species. The relativistic correction factor η is

$$\eta = \frac{2T_e}{m_o c^2} + \frac{2}{Z_{eff}} \left(1 - \frac{1}{(1 + \frac{T_e}{m_o c^2})^2}\right) \tag{17}$$

where $m_o c^2$ is the rest mass energy of the electron.

The electron-ion rethermalization power is given by

$$P_{ie} = \frac{3 \times 10^{-12} n_e}{T_e^{3/2}} \left(\sum_j \frac{n_j Z_j^2}{A_j}\right) (T_i - T_e) \delta \tag{18}$$

where δ is a relativistic correction factor given by[2]

$$\delta = 1 - 0.3 \frac{T_e}{m_o c^2} \quad . \tag{19}$$

Let us now use eqn. (14), (15) and (18) to estimate Q for the p-^{6}Li cycle. We will include the ^{3}He density from eqn. (13) in estimating Z_{eff} but we do not include the ^{3}He-^{3}He fusion reactions. Work on this is in progress.

The fast protons produced from ^{3}He-^{6}Li reactions will give energy to both electrons and ions. At 12 MeV, the coulomb cross section has become small and p-p elastic scattering is likely to dominate. This would imply that the protons would heat ions and could produce additional fast protons as discussed previously. However, since the analysis of this effect is in progress, we consider here two cases. In case 1, it is assumed that all fusion energy goes to the ions. In case 2, it is assumed that 80% of fusion energy goes directly to electrons and only 20% to the ions. Some

typical results for case 1 are summarized on Table 2. The parameter γ is n_6/n_1. One notes immediately that ignition may be possible. For the case T_i = 300 keV and γ = 0.5 (33% ^{6}Li, 66% p), the fusion power balances electron drag at T_e = 110 keV. The ratio of fusion power to bremsstrahlung, P_F/P_X, is then 3.5 which means the power margin over ignition is 2.5 P_X. This can be translated into a minimum $n_e\tau_E^e$ for the electrons such that P_F will just balance all electron losses. For the case under discussion, $(n\tau_E^e)_{min}$ = 5.7 x 10^{14}xm^{-3}-s. As T_i increases, the margin over ignition continues to improve such that $(n\tau_E^e)_{min}$ decreases to 1.4 x 10^{14}cm^{-3}-s.

Results for case 2 are summarized on Table 3. Since 80% of the fusion power goes to the electrons, the equilibrium values of T_e are higher. The optimum γ is 0.7 where, for T_i = 300 keV, we find $T_e \simeq$ 150 keV, $P_{16} \simeq$ 0.88, and the margin against ignition is ~20 P_X. Since T_e has increased, the minimum $n_e\tau_E^e$ at which the energy into the electrons balance all electron losses is still about 1.4 x 10^{14}cm^{-3}-s. Nevertheless, these margins over ignition are substantial.

These results differ from those of Cordey[2] because we consider all generations in the chain reaction and find P_{16} is greater than 0.5 when $T_e \gtrsim$ 100 keV. By neglecting the chain reaction effect and assuming that the reactivity is only enhanced by $(Q_{16}+Q_{36})(1+P_{16})$, we too would find, as did Cordey, that p-^{6}Li would not ignite. The fact that it may ignite, and the fact that the margin beyond ignition can be significant makes this essentially neutronless fuel cycle of extreme interest for further investigation.

IV. Multipoles as Reactors for Advanced Fuels

We have seen that advanced fuel cycles, and particularly p-^{6}Li, will require a relatively high electron temperature (>50 keV). It is clear that

Table 2

Case 1 (All fusion power deposited in ions)

T_i	T_e	γ	P_{16}	P_F/P_{ei}	P_F/P_x	$(n\tau_e)_{min}$
300	130	.2	.611	1.043	2.485	1.16×10^{15}
	120	.3	.662	1.142	2.734	9.23×10^{14}
	110	.4	.673	1.035	3.389	6.38×10^{14}
	110	.5	.710	1.158	3.545	5.74×10^{14}
400	140	.2	.648	1.063	3.263	7.45×10^{14}
	125	.3	.683	1.060	4.01	5.25×10^{14}
	120	.4	.717	1.155	4.603	4.27×10^{14}
	115	.5	.733	1.131	4.75	3.99×10^{14}
500	130	.2	.616	1.050	3.972	5.59×10^{14}
	130	.3	.704	1.125	5.231	7.06×10^{14}
	120	.4	.72	1.072	5.673	3.232×10^{14}
	115	.5	.735	1.055	5.88	1.44×10^{14}

Table 3

Case 2 (80% of Fusion Power to Electrons)

$\gamma = \frac{n_6}{n_1}$	T_i	T_e	P_{16}	$.2P_F/P_{ei}$	P_F/P_x	$(n_e\tau_E^e)_{min}$
.2	300	190	.780	1.007	5.68	5.815×10^{14}
.2	400	210	.820	1.045	7.667	4.557×10^{14}
.2	500	220	.830	1.007	9.544	3.502×10^{14}
.3	300	175	.828	1.130	8.084	4.434×10^{14}
.3	400	185	.849	1.029	11.576	2.814×10^{14}
.3	500	190	.860	1.003	13.4619	2.264×10^{14}
.4	300	165	.850	1.151	9.595	3.454×10^{14}
.4	400	170	.862	1.058	12.633	2.525×10^{14}
.4	500	180	.882	1.110	17.095	1.787×10^{14}
.5	300	155	.856	1.022	10.213	3.150×10^{14}
.5	400	165	.879	1.040	14.077	2.200×10^{14}
.5	500	170	.890	1.070	18.575	1.619×10^{14}
.6	300	155	.876	1.171	11.079	2.852×10^{14}
.6	400	160	.887	1.028	14.685	2.076×10^{14}
.6	500	165	.898	1.053	19.506	1.518×10^{14}
.7	300	150	.879	1.079	11.095	2.830×10^{14}
.7	400	160	.901	1.042	15.655	1.902×10^{14}
.7	500	160	.902	1.022	20.829	1.405×10^{14}
.8	300	150	.89	1.152	11.421	2.694×10^{14}
.8	400	155	.901	1.070	16.497	1.793×10^{14}
.8	500	160	.912	1.138	20.610	1.400×10^{14}
.9	300	145	.889	1.017	11.128	2.780×10^{14}
.9	400	155	.910	1.106	15.792	1.855×10^{14}
.9	500	155	.911	0.994	19.950	1.450×10^{14}

synchrotron radiation losses, when coupled with the large emission due to bremsstrahlung, would prevent a positive reactor energy balance. Therefore, it is necessary to minimize or eliminate synchrotron emission by eliminating the magnetic field from the bulk of the plasma.

Octopoles and higher order multipoles are confinement approaches which have this property. Dawson[1] has shown that octopoles and higher order multipoles may be feasible if confinement times continue to follow the observed scaling found by Post, Navratil and Kerst in the University of Wisconsin octopole.[5-7] As such, it is important to examine an octopole as an advanced fuel cycle fusion reactor to more rigorously access requirements, to suggest important experimental directions for the octopole program, and to suggest further directions in a reactor feasibility study. We describe here preliminary considerations regarding this topic. The plasma parameters for a typical reactor size device are listed on Table 4. The major radius is 7m and the effective plasma radius (to the β=1 boundary) is about 1.5 m. The β in the bridge region where ballooning modes are of greatest concern is 20% and the plasma power density is about 4.4 MW/m^3. The parameters for this octopole plasma have been obtained by straightforwardly scaling the dimensions of the Wisconsin octopole. A schematic cross section view of the system is shown in Fig. 8.

The reactor is toroidal with four current-carrying hoops. The main field is the poloidal field and only a weak toroidal field (~5 kG) is required. In addition, the octopole hoops will be superconducting and no transformer core is required. Thus, unlike tokamak systems, one has significant access space near the centerline of the device and the toroidal field coils do not dominate the design, either in physical dimension or in cost. The

Table 4

Parameters for a p-^{6}Li Octopole Fusion Reactor

B_{max}	50 kG	R	7m
β (Bridge)	20%	a_p (effective)	1.5m
T_e	150 keV	R_i (inner hoop)	5m
T_i	300 keV	R_o (outer hoop)	9m
$n\tau_E^e$	2.8×10^{14} cm^{-3}-s	Thermal Power	1370 MW_{th}
$\gamma=n_6/n_1$	0.7	Q	(Ignition)
n_p	6×10^{13} cm^{-3}		
P_{16}	0.88		
Power Density	4.4 W/cm^3		

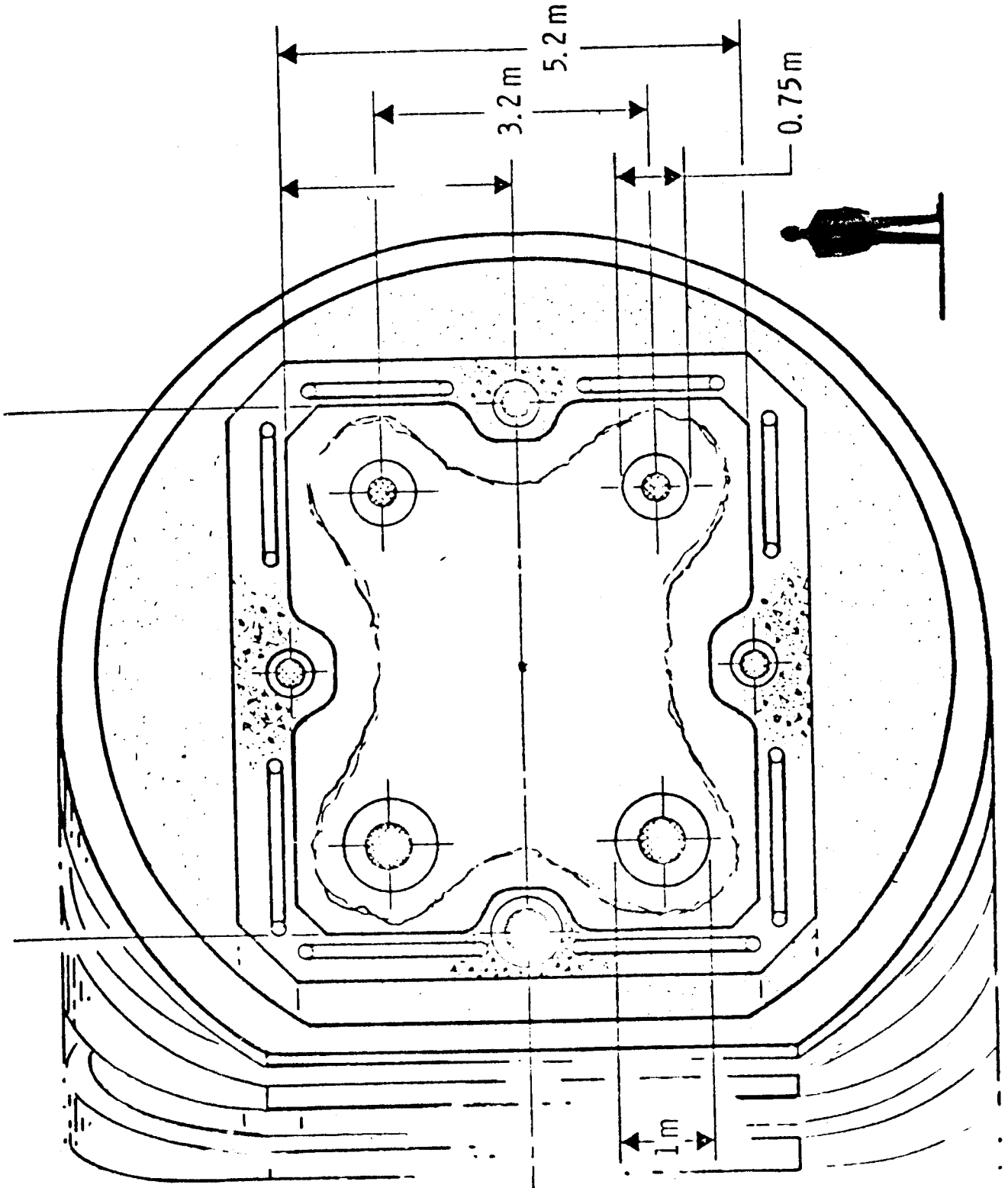

FIGURE 3

coils shown outside the vacuum chamber are to levitate the four internal octopole rings.

A. Octopole Coil Design

The design of the four internal current hoops is one of the major technological aspects of octopole reactors. These coils must be superconducting to eliminate power losses and levitated to minimize or eliminate supports. We consider first the design of the conductor itself and then turn to coil cooling considerations. The maximum field on the surface of the inner hoop is 5T. The assumption is made that the coils will not be built to withstand the magnetic loading but rather that external coils, built into the structure, will be used to both levitate the coils and to cancel the magnetic loading. This, of course, implies that special precautions must be taken to ensure that the current in any of the coils does not come on without the corresponding current in the force-cancelling coil coming on simultaneously.

For a cryogenically stable coil operating in a 5T field, an overall current density of 3000 A/cm^2 is reasonable. We have also selected a 20% void fraction for liquid helium. A 3 cm zone is provided between the liquid helium barrier and the outer coil surface. (There may be a material with a large heat capacity, such as Pb, around the outside of the coil to provide thermal capacity at cryogenic temperatures.)

The self field at a radius R from a solenoid is given by

$$B_o = \frac{\mu_o I}{2\bar{n} R}$$

where B_o is in Tesla, μ_o for air vacuum is $4\bar{n} \times 10^{-7}$, I is in amperes and R is in m. Taking a 20% void fraction and an average current density of

3×10^7 A/m^2, we have

$$\frac{I}{\pi r^2 (1.2)} = 3 \times 10^7 \text{ A/m}^2.$$

Combining the two equations gives

$$B_o = \frac{\mu_o (3 \times 10^7)(\pi R^2)(1.2)}{2\pi R}$$

For R = r + 0.03, we find r = 0.25 m and I = 7 MA. Similarly, the outer hoop, which will have a maximum field of 2.33T is found to have a radius of 0.1 m and a current of 1.5 MA. The overall current density in the outer hoop is taken as 4×10^7 A/m^2 since it is in a lower field.

The conductor selected is one designed by Cornish at Lawrence Livermore Laboratory. The Cornish conductor employs work-hardened copper as both stabilizer and structure. To provide maximum cooling surface, each conductor is manufactured in four pieces as shown in Fig. 9 and then soldered together. The superconducting filaments are contained in one piece only and are twisted and transported during manufacture. Two of the remaining three pieces can have 1 mm grooves machined over one-half of the surface in contact with the other conductors in order to provide internal cooling chambers. The four copper conductors are also leveled to provide additional passages for the coolant. During winding, the conductor is wrapped in a spiral fashion over half of its area such that in the coil, the conductor will be separated by 1 mm of fiber glass epoxy insulation.

Fig. 10 shows a cross section of an inner coil. The square blocks represent the conductors (not shown to scale for clarity) separated by insulation. The conductors are banded with split rings which are fastened at the midplane by bolts. These bands are 5 cm wide and are placed at

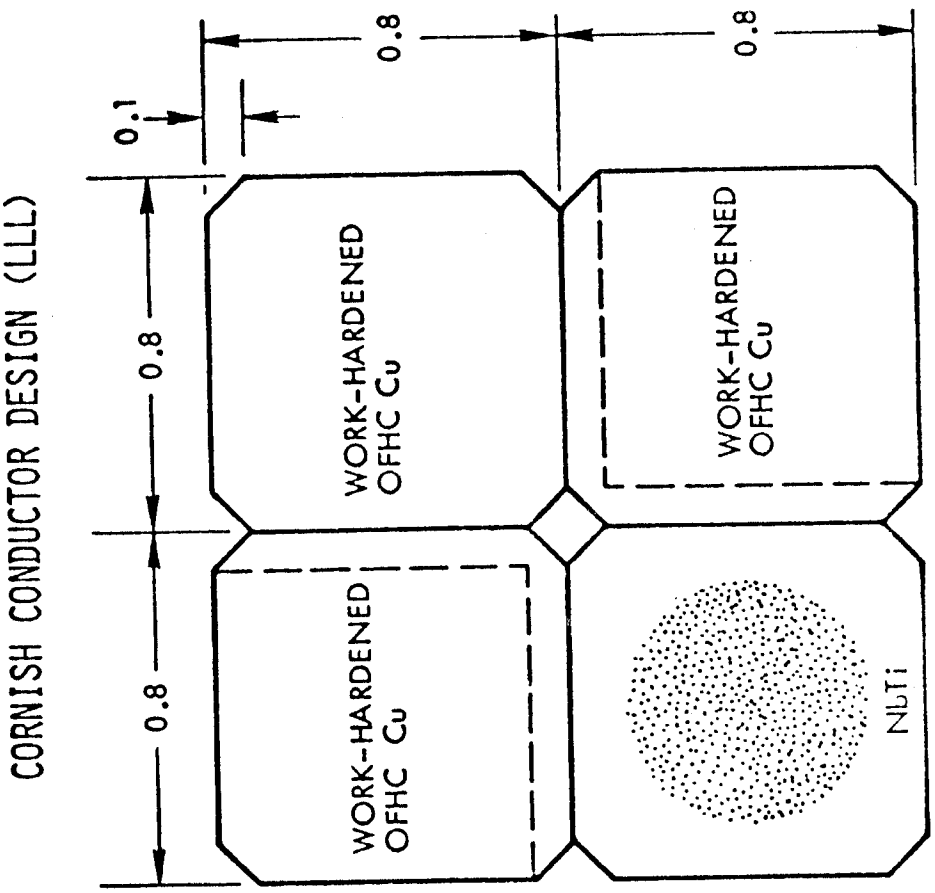
CORNISH CONDUCTOR DESIGN (LLL)
0.1
0.8
0.8
0.8
0.8
WORK-HARDENED
OFHC Cu
WORK-HARDENED
OFHC Cu
WORK-HARDENED
OFHC Cu
NbTi

FIGURE 9

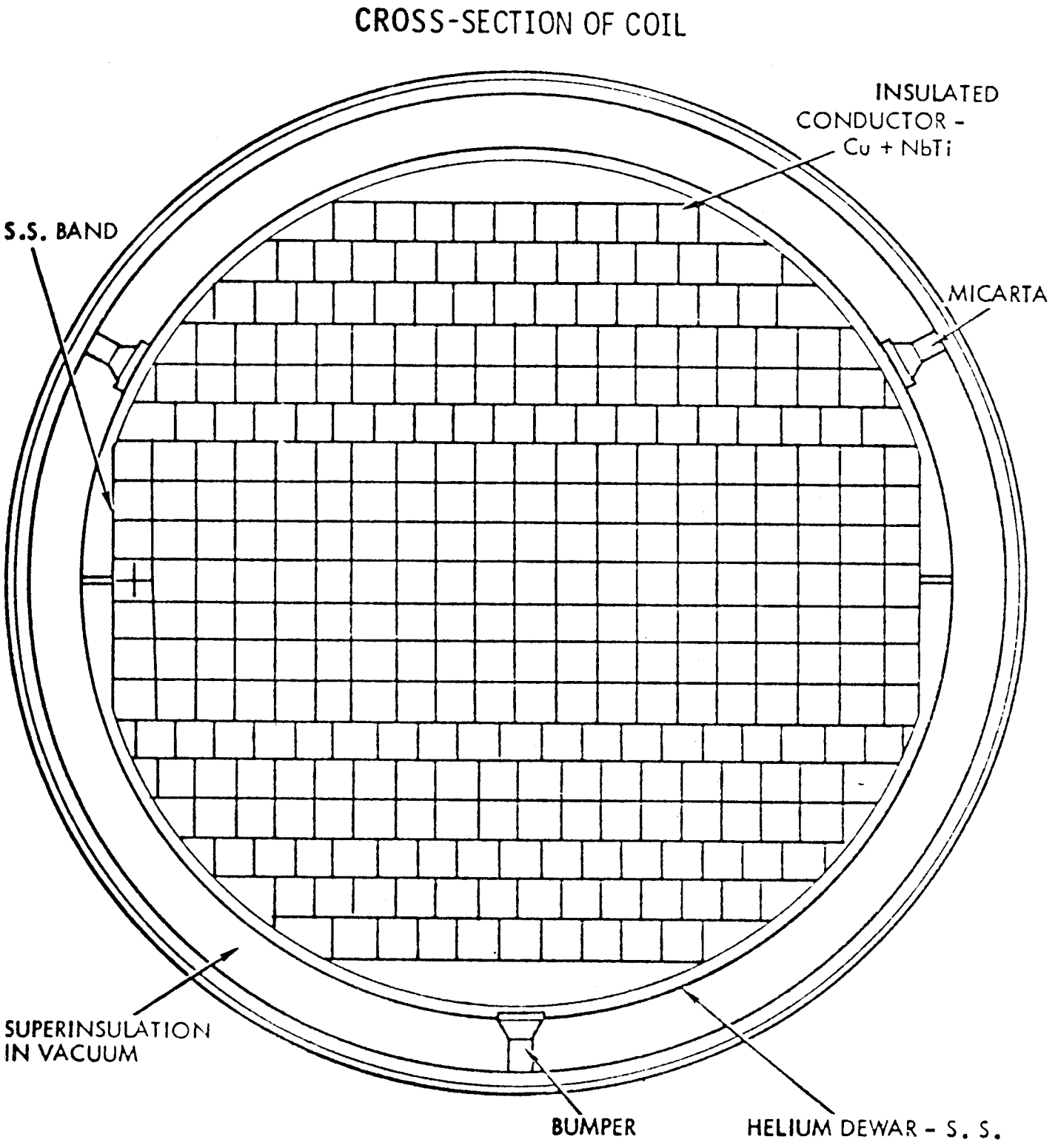
CROSS-SECTION OF COIL
INSULATED
CONDUCTOR -
Cu + NbTi
S.S. BAND
MICARTA
SUPERINSULATION
IN VACUUM
BUMPER
HELIUM DEWAR - S. S.

FIGURE 10

one-meter intervals. Micarter spacers would be used to fill in the voids at the layer terminations and to electrically insulate the bands from the conductor.

Since the outer surface of the bands is circular and smooth, the liquid helium dewar can be assembled right on top of them or on top of Pb if it is required. Sections of the dewar can be placed in semi-toroidal configuration with the seam coming together at the midplane. Welding the two halves together and adjacent sections circumferentially will seal the liquid helium dewar. If the helium dewar is made of 1-mm thick 316 SS, it can withstand an internal pressure of 13 atm. This is important in the event the coil goes normal and the liquid helium evaporates rapidly.

The helium dewar is separated from the vacuum vessel by 3 cm with fiberglass epoxy bumpers that are 1 cm^2 in cross section. The effective thermal conductivity of the bumpers is taken as 0.0034 W-cm-°K. A summary of the parameters characterizing the coils is given on Table 5. One should note that this design, while quite feasible, is conservative and one should consider using Nb_3Sn for this application because of its higher critical temperature. At the fields required, this should pose no extreme difficulty.

The octopole coils are imbedded in the plasma and are therefore subject to an intense surface heat load. The two possibilities for cooling are listed on Table 6. Levitating the coils but allowing small leads to carry an external coolant has been examined. It is found that incident heat loads of approximately 100 W/cm^2 can be removed using 4 to 8 coolant leads per hoop. The cross section presented to the plasma would be 3-6 cm times the length of the lead. An actively cooled hoop offers the potential for steady

Table 5

Parameters of Octopole Reactor Coils

	Inner Coils	Outer Coils
Max. Field (kG)*	50	23.3
Coil Current (MA)	7	1.5
Major Radius (m)	5	9
Minor Diameter (m)	0.56	0.26
Superconductor**	NbTi	NbTi
Stabilizer**	Cu	Cu
Current Density (A/cm^2)**	3000	3000
Superconductor/Cu Ratio	1:33	1:40
Mass of Cu/coil (ton)	43	12.4
Mass of NbTi/coil (ton)	1	0.25

** S/C could be Nb_3Sn. Stabilizer could be Al. Current density could be raised to 5000 A/cm^2

* Fields corrected to be uniform around coil.

Table 6

Coil Cooling

Two Cases:

1. Levitated but with coolant leads.

Result: Coil can be run steady state. Lead cross section seen by plasma is ~3-6 cm x height. Probably require 4-8 coolant leads/hoop.

2. Levitated and with coolant leads.

Result: Coil operating time is limited but can be long (50 hours or more, depending on design).

state operation but a simple calculation shows that such leads, if unprotected, would be subject to enormous heat loads, to say nothing of the effect such losses would have on confinement. Thus, magnetic guarding will be essential if leads are used. Guarded leads have been tried experimentally on the quadrupole at Los Alamos Scientific Laboratory and to some extent on octopoles but much further work is required. Such experiments can be done in present and future machines.

The other possibility is to design levitated coils with a large thermal capacity such that days of continuous operation are possible without external cooling. The generic design for such a coil is shown in Fig. 11. An estimate of the surface heat load to the coil exterior is approximately 100 W/cm^2. The outer wall must therefore be designed for high reflectivity and operation at about 2000°K. The central superconducting coil, on the other hand, is 4 to 20°K. To minimize the heat leak, one requires three additional zones, a super-insulating zone around the cryogenic coil, a zone of high thermal capacity (high ρ Cp) that operates up to several hundred °C, and a zone of high temperture insulation. (In practice, the detailed design of each general zone may consist of several zones and different materials. The net effect, however, would be to achieve values of thermal conductivity about equal to those given on Fig.11.) The middle zone of high ρ Cp and relatively low melting temperature, T_m, serves the dual purpose of separating the low and high temperature insulating zones while providing a heat sink within the coil. A convenient material for the middle zone is lithium. One would begin with the Li at 77°K and allow it to heat to its melting point of 459°K and to melt. In this way, the enthalpy consists of both the temperature rise and the heat of

GENERIC DESIGN FOR A LEVITATED OCTOPOLE COIL WITHOUT EXTERNAL COOLING

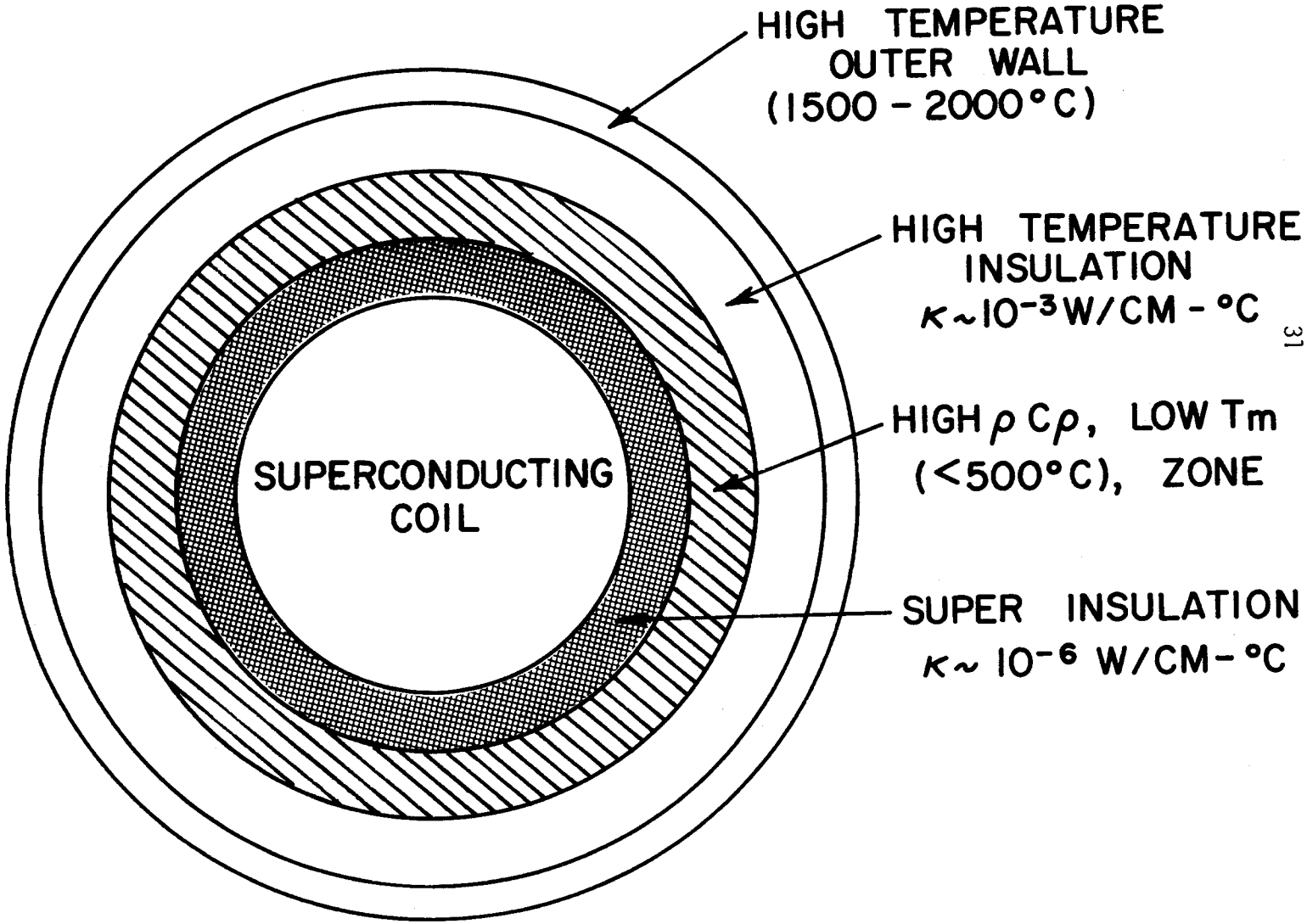

Figure 11

melting. In addition, the very small neutron flux from side reactions will be further reduced at the superconductor, stabilizer, and superinsulation.

The simple planar calculation outlined on Fig. 12 shows that with the lithium zone and high temperature insulating zones each at 22 cm, the time to melt all the lithium is 50 hours. Over this period, the heat leak to the superconducting bath is only 15 W. Using Pb in the superconducting zone as a heat sink and/or allowing the temperature to rise to perhaps 12-15°K by using Nb_3Sn means the time to melt the Li is the shortest time constant. Thus, with quite reasonable zone thicknesses, two or more days of continuous operation are possible. Therefore, this design approach seems feasible and should be examined in greater detail.

B. Power Cycle Considerations and Plasma Q Values

The lack of neutrons means radiation damage is not a factor in choosing either structural materials or coolant operating temperatures. It is thus more reasonable to consider power cycles that can have high thermal cycle efficiency. All of the fusion reaction energy is deposited in the plasma and subsequently radiated to the first wall. In essence, therefore, a p-^{6}Li octopole reactor is the fusion equivalent of a coal-fired boiler. The thermal efficiency possible with different power cycles is shown in Fig. 13. The potassium topping cycle system is attractive and has been the subject of research by Fraas at the Oak Ridge National Laboratory. We have considered this approach for an octopole reactor and assumed that the operating temperature of the first wall is 1000°C. The resulting power cycle is shown on Fig. 12 and the gross electrical output from each turbine system is summarized on Table 7. The gross cycle efficiency is 54%.

TYPICAL COIL DESIGN ANALYSIS

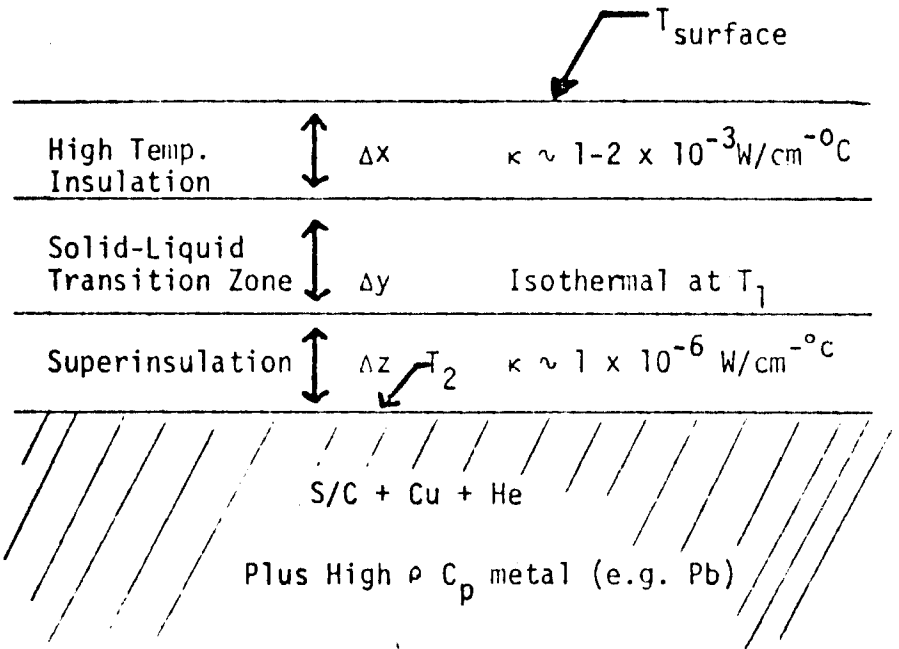

Example: Solid-Liquid Zone is Lithium
(Initially at 77°K; T_m = 459°K)

Total Enthalpy of Li = 210 Δy cal/cm^2

Heat Flow Inward (T_s = 2000°K) $\simeq \frac{0.575}{\Delta x}$ cal/cm-s

Time to melt all Li $\sim$ 365 Δx Δy (s)

For $\Delta x = \Delta y$ = 22 cm, Time = 50 Hours

For Δz = 10 cm, Heat Leak to S/C $\simeq$ 15 W

FIGURE 12

COMPARISON OF TYPICAL THERMAL EFFICIENCIES FOR REPRESENTATIVE THERMODYNAMIC CYCLES

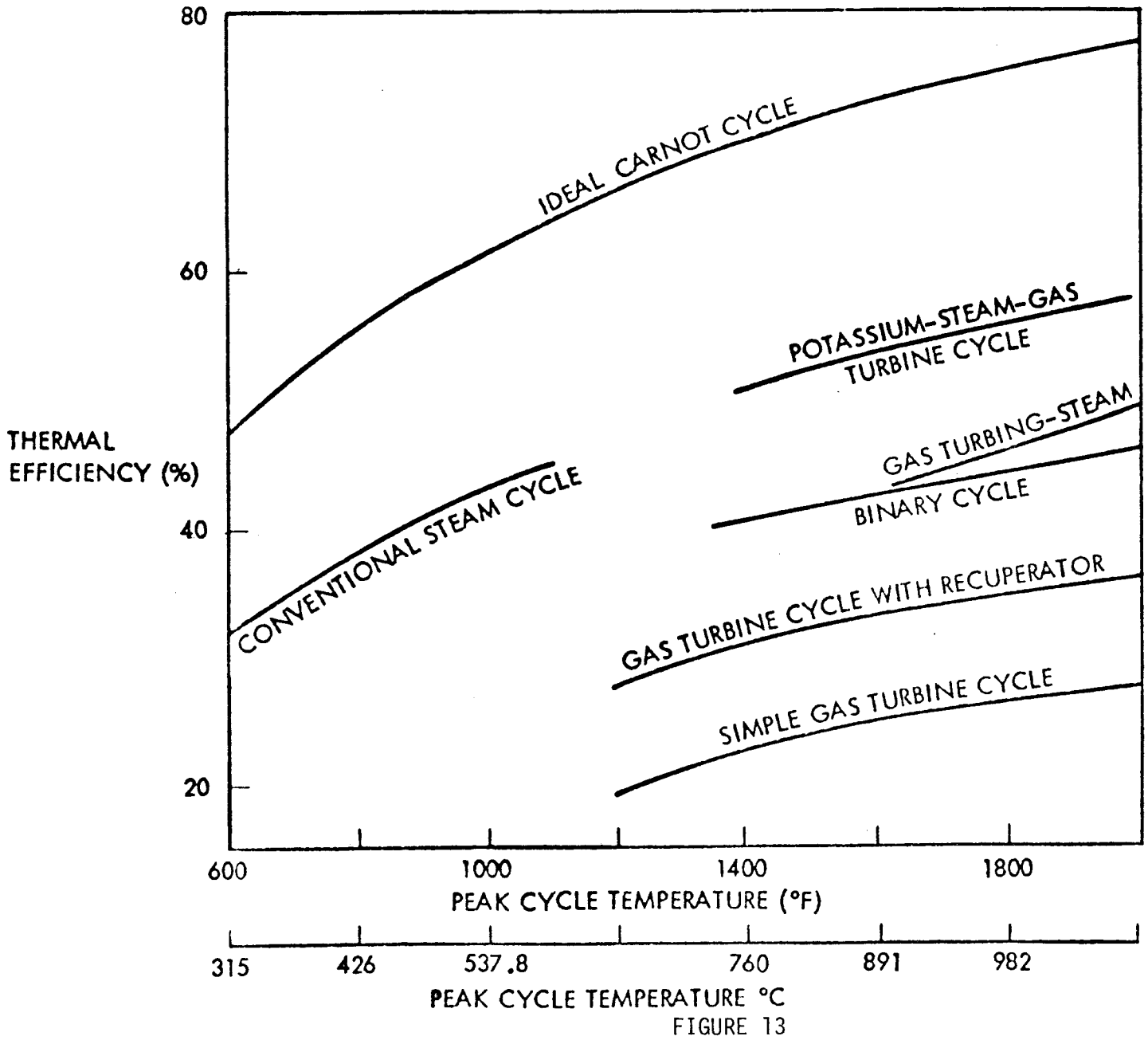

FIGURE 13

FLOW DIAGRAM FOR K-TOPPING CYCLE

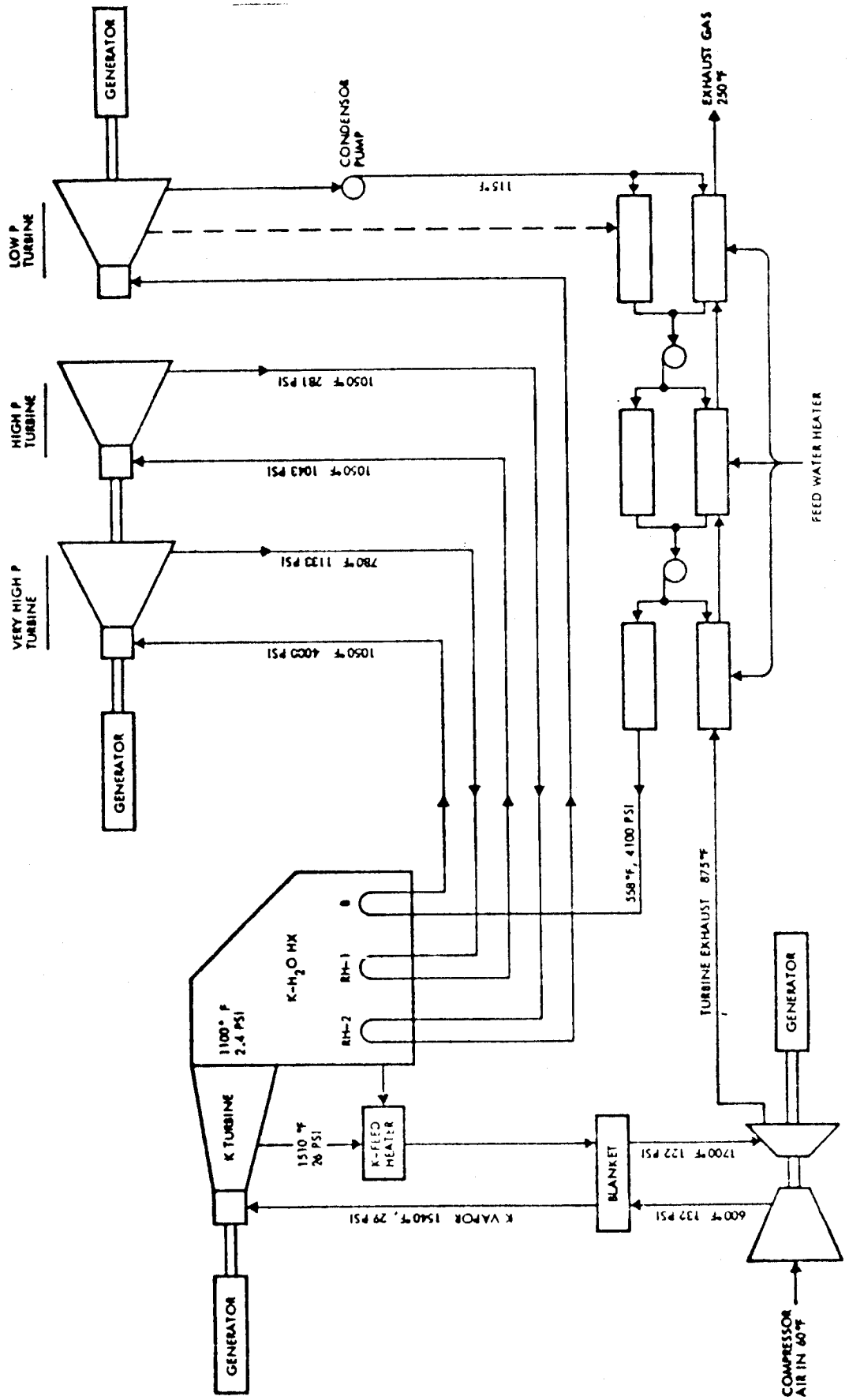

FIGURE 14

Other advanced notions may be possible with neutronless fuel cycles. For example, the bremsstrahlung radiation can be transmitted through a low Z first wall and stopped in a clean gas to be used as the working fluid in an MHD cycle. Advantages here would be the lack of mineral impurities associated with coal-derived gases and cycle efficiencies of 65-70%.

An alternate approach to the question of cycle thermal efficiency is to ask what gross efficiency, η_{th}, and what plasma amplification factor, Q, are required to produce a plant of acceptable net thermal efficiency, η_{net}. A quite simple power balance relating Q, η_{th}, and η_{in}, where η_{in} is the power injection efficiency,gives

$$\eta_{net} = \eta_{th} - \frac{1}{\eta_{in}(Q+1)}$$

where η_{net} is the net cycle thermal efficiency, i.e., the net electrical output divided by the total thermal power. Taking a net plant efficiency of 30% as a rough indicator of economic breakeven, (i.e., utilities are unlikely to be interested in power stations with much lower efficiencies), one requires plasma amplification factors between 4 and 6 when η_{th} = 54% if the injection power efficiency is between 70 and 80%. Interestingly, this is similar to the Q value and injector energy and efficiency requirements of the tandem mirror concept recently developed in the U.S. and U.S.S.R. Higher Q values in the range of 10 are required if η_{in} is 50%. From the plasma physics considerations discussed in section III, ignition against bremsstrahlung appears feasible with p-^{6}Li so that Q values greater than 5 is certainly a strong possibility.

Table 7

Power Cycle Analysis

Thermal Power	1370 MW
Gross Electrical Output	
Gas Turbine	92 MW
K Turbine	156 MW
Steam Turbine	497 MW
Total Gross Electrical Output	745 MW_e
Gross Cycle Efficiency	54%

V. Future Directions in Experiments and Physics Suggested by Reactor Considerations

The preceding reactor analysis, preliminary though it is, has suggested important physics information required to make an improved assessment of advanced fuel cycle multipole fusion reactors. These are summarized on Tavle 8 and a number of topics can be studied on a near term proof of principle experiment. Clearly, the scaling of the diffusion coefficient, $D_{\perp}$, and the plasma thermal conductivity, κ, with machine size, plasma collisionality, and β are critical. The favorable scaling observed for $D_{\perp}$ in the UW octopole is quite encouraging here. Impurity effects and alpha particle diffusion are very important for reactors and will probably determine the longest feasible burn time.

Leads to hoops can change the concept of an octopole reactor so the effects of hoop leads on diffusion and methods for guarding leads are both important. An experiment should be designed fully levitated to allow both modes of operation. Also, we found earlier that the self-field of each current hoop is very large in reactor size machines. (Some of the coils are in tension while others are in compression, even when the hoops are fully levitated.) It is therefore necessary to use external trimming coils to eliminate these self forces and the effects of this on confinement is an important physics question.

Finally, one should recognize that a sequence of devices will be involved in reaching an advanced fuel cycle reactor. A proof-of-principle experiment (POP) using hydrogen is the logical next step. The plasma parameters will be in the range, $n \sim 10^{13}$-10^{14} cm^{-3}, $T \sim 1$ keV. The next device, say POP-II,

Table 8

Physics Information Required for an Improved Assessment of p-^{6}Li Multipole Reactors

- Improved ^{3}He-^{6}Li and ^{3}He-^{3}He Fusion Cross Sections from 100 keV to 10 MeV.
- Scaling of $D_{\perp}$ and κ* (Scaling of $n\tau$)
- Finite Beta Plasma Behavior*
- Alpha Particle Diffusion
- Impurity Effects and Control*
- Effects of Hoop Leads on Diffusion
- Methods for Guarding Leads*
- Effect on Confinement of Making B Uniform Around a Hoop*
- Cross Sections and Branching Ratios of Neutron Producing Side Reaction
- Bremsstrahlung and Synchrotron Losses in High Temperature Octopoles

* Topics Which Can Be Studied in a Near Term Proof-Of-Principle Experiment

will be aimed at achieving Q=1 with an advanced fuel and at the study of the physics of advanced fuel burn dynamics. As we have shown, D-^{3}He can achieve Q=1 at T_i ~ 50-75 keV, T_e ~ 30-40 keV. It is the fuel of choice for the POP-II machine, Results from these devices then provides a foundation to proceed to a truly p-^{6}Li advanced fuel cycle test reactor at high Q.

References

1. J. M. Dawson, "CTR Using the p-^{11}B Reaction" UCLA Plasma Group Report, PPG-273 (Aug. 1976).

2. J. G. Cordey, "Hot Ion Toroidal Reactors and Exotic Fuel Cycles", Lecture 2. Course on Theory of Magnetically Confined Plasmas (Varenna, Italy) Sept. 1977.

3. R. W. Conn et al., "Aspects of Octopoles as Advanced Cycle Fusion Reactors" IAEA Meeting on Fusion Reactor Design (Madison, WI) Oct. 1977. To be published by IAEA.

4. J. R. McNally, Jr., Nucl. Fusion 11 (1971) 187-193.

5. J. R. Drake, J. R. Greenwood, G. A. Navratil, R. S. Post, Phys. Fluids 20, 148 (1977).

6. G. A. Navratil, R. S. Post, Phys. Fluids 20, 1205 (1977).

7. ibid. Bull. Am. Phys. Soc. 22, 1151 (1977).